Check for updates

Geophysical Research Letters

RESEARCH LETTER
10.1029/2024GL112500

Transient Deformation in the Tatun Volcano Group, Taiwan: A Spatiotemporal GPS Analysis

Yi-Sheng Huang[1,2], Wu-Lung Chang[1,3], Hsin-Chieh Pu[4], Chi-Yu Chiu[1,3], Ya-Chuan Lai[5], and Min-Hung Shih[5]

[1]Department of Earth Sciences, National Central University, Taoyuan, Taiwan, [2]Institute of Earth Sciences, Academia Sinica, Taipei, Taiwan, [3]Earthquake Disaster & Risk Evaluation and Management Center, National Central University, Taoyuan, Taiwan, [4]Central Weather Administration, Taipei, Taiwan, [5]National Center for Research on Earthquake Engineering, NARLabs, Taipei, Taiwan

Key Points:

- Data-adaptive detection of transient deformation in noisy GPS time series
- Cycle of ground deformation first detected in the Tatun Volcano area, where about 7 million people reside nearby
- Hydrothermal processes may have driven consistent spatiotemporal variations in seismicity and deformation in the Tatun Volcano area

Supporting Information:

Supporting Information may be found in the online version of this article.

Correspondence to:

W.-L. Chang,
wuchang@ncu.edu.tw

Citation:

Huang, Y.-S., Chang, W.-L., Pu, H.-C., Chiu, C.-Y., Lai, Y.-C., & Shih, M.-H. (2024). Transient deformation in the Tatun Volcano Group, Taiwan: A spatiotemporal GPS analysis. *Geophysical Research Letters*, *51*, e2024GL112500. https://doi.org/10.1029/2024GL112500

Received 17 SEP 2024
Accepted 27 NOV 2024

Author Contributions:

Conceptualization: Wu-Lung Chang
Data curation: Hsin-Chieh Pu, Chi-Yu Chiu, Ya-Chuan Lai, Min-Hung Shih
Formal analysis: Yi-Sheng Huang, Chi-Yu Chiu, Ya-Chuan Lai, Min-Hung Shih
Funding acquisition: Wu-Lung Chang
Investigation: Wu-Lung Chang
Resources: Wu-Lung Chang
Software: Yi-Sheng Huang
Supervision: Wu-Lung Chang
Validation: Yi-Sheng Huang, Wu-Lung Chang, Hsin-Chieh Pu
Writing – original draft: Yi-Sheng Huang
Writing – review & editing: Wu-Lung Chang, Hsin-Chieh Pu

© 2024. The Author(s).
This is an open access article under the terms of the Creative Commons Attribution License, which permits use, distribution and reproduction in any medium, provided the original work is properly cited.

Abstract This study analyzed time series data from six GPS stations within the Tatun Volcano Group (TVG), a long-dormant volcanic system in northern Taiwan, using multichannel singular spectrum analysis to search for potential spatiotemporally correlated transient deformations. A notable cycle of transient deformation was identified from 2015 to 2020, characterized by ground subsidence and uplift of up to 10 mm, accompanied by asymmetric horizontal motions directed inward and outward toward Dayoukeng, the largest fumarole and hydrothermal area in TVG. Evidence from earthquake focal mechanisms and gas composition, along with preliminary source modeling, suggest that these transient phases were likely caused by the pressure change of shallow hydrothermal systems beneath Dayoukeng. Further analysis of time series data from three long-operating GPS stations revealed similar patterns of transient motion in the area from 2006 to 2015, indicating that TVG has experienced cyclical deformation, akin to many other volcanic systems worldwide.

Plain Language Summary Monitoring ground deformation in volcanoes is crucial for understanding the underlying processes and providing early warnings of potential hazards. Previous geodetic studies of the long-dormant Tatun Volcano Group (TVG) in northern Taiwan relied on sporadic data, leading to incomplete insights into its time-varying deformation behavior. Continuous GPS, however, allows for accurate tracking of surface movements over time, including short-term changes caused by intermittent volcanic activity. This first GPS study of TVG employed a method called multichannel singular spectrum analysis to identify transient signals in noisy data from six stations. Significant ground deformation was revealed between 2015 and 2020, with the ground sinking and rising by up to 10 mm, along with horizontal movements toward and away from Dayoukeng, a major steam vent area in TVG. This sinking is likely related to changes in the shallow hot water and steam systems beneath Dayoukeng, as suggested by anomalies in earthquake activity and surface gas composition. Additional GPS data from 2006 to 2015 revealed that TVG experienced recurring cycles of ground deformation, closely correlated with local seismic activity.

1. Introduction

The Tatun Volcano Group (TVG) covers an area of ~400 km^2 in northern Taiwan, comprising over twenty Quaternary volcanoes (Chen et al., 2007) and the Miocene active Shanchiao normal fault that straddles the area (Figure 1). Although there hasn't been a recorded eruption in recent history, volcanic activity is still evident through features such as hot springs and fumaroles. Give the proximity of the Taipei metropolis, home to ~7 million people, and two nuclear power plants (Figure 1), the Taiwan Volcano Observatory at Tatun (TVO) has monitored volcanic activity since the early 2000s using various instruments. Numerous evidence such as dense micro-earthquakes (Pu, Lin, Lai, et al., 2020), composition of emitted volcanic gases (Lee et al., 2008; Yang et al., 1999), and seismic images of magma reservoir (H.-H. Huang et al., 2021; Lin, 2016) suggest that the area is experiencing ongoing volcanic activities.

Despite several geodetic measurements conducted in and around the TVG, transient ground deformation in this area has not been extensively studied. Murase et al. (2014) conducted precise leveling surveys from 2006 to 2013 around Mt. Cising and the Dayoukeng fumarole, areas known for frequent earthquake swarms and abundant hydrothermal activity in the TVG region (Figure 1). They observed episodes of ground uplift and subsidence during this period, with amplitudes reaching up to 10 mm, and proposed a two-spherical-source model to represent shallow hydrothermal reservoirs responsible for the transient deformation. Tung et al. (2016) calculated

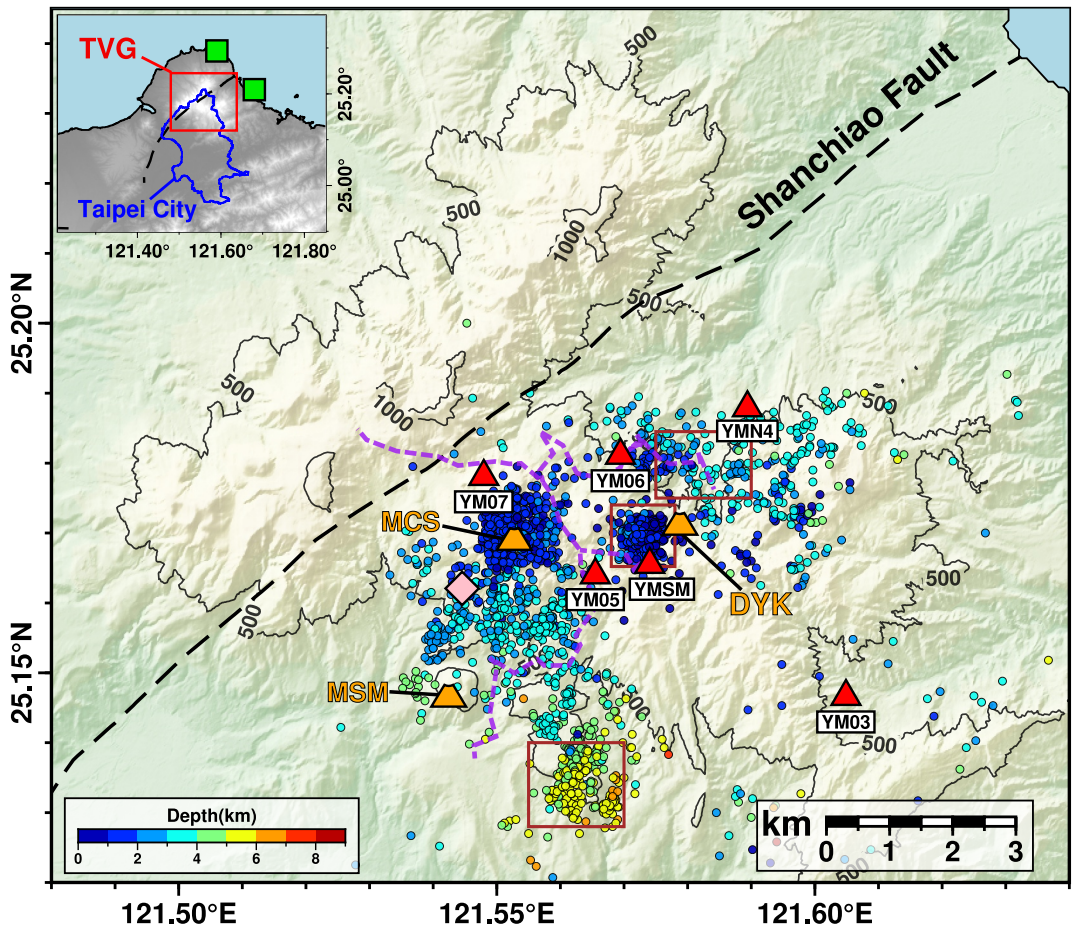

Figure 1. Map showing the Tatun Volcano Group (TVG) area and the six GPS stations used in this study (red triangles). Orange triangles mark volcanic features mentioned in this study: Mt. Cising (MCS), the Dayoukeng fumarole (DYK), and Mt. Shamao (MSM). Purple dashed lines represent leveling survey routes in Murase et al. (2014). Color circles show 2014–2017 relocated seismicity in Pu et al. (2021a), with the three rectangles representing, from north to south, the January 2019 (Peak 4), October 2009 (Peak 1) and April–June 2015 (Peak 3), and February 2014 (Peak 2) sequences (see Figure 4a and the main text). The pink diamond marks the Zhuzihu weather station, and two green rectangles in the insert label nuclear power plants.

the horizontal ground motion using 14 GPS stations in the Taipei metropolitan area and identified a WNW–ESE extensional principal strain rate of 0.28 μstrian/yr near TVG. By integrating data from 112 GPS stations (both continuous and campaign modes) with 43 InSAR images in northern Taiwan, Chang et al. (2017) observed episodes of subsidence (2003–2008) and uplift (2007–2011) with average rates reaching up to ∼4 mm/yr and a principal strain rate of 0.23 μstrian/yr in the TVO area, despite the InSAR data being noisy and sparse.

While several continuous GPS stations have been operated in TVG for monitoring volcanic unrest, ground deformation caused by volcanic activity in this area can be too localized and subtle to be detected through GPS time series. In fact, numerous challenges can arise when attempting to detect short-term transient ground motions using this method. First, most transient signals exhibit non-linear trends that cannot be easily modeled using traditional least-squares fitting of simple analytical functions like linear trends and periodic components (e.g., Nikolaidis, 2002). Second, temporally and spatially correlated noise in GPS time series could obscure signals (e.g., Bos et al., 2013; Langbein, 2017). Lastly, visually inspecting each time series in a GPS network for common transient signals is time-consuming and potentially unreliable. These factors may cause the relatively low ground deformation signals from volcanic activity to go unnoticed.

While various complex processes can interact to cause transient ground deformation, such motion often appears as nonlinear cyclical trends in GPS time series common to multiple stations in a volcanic area (e.g., Chang

19448007, 2024, 24, Downloaded from https://agupubs.onlinelibrary.wiley.com/doi/10.1029/2024GL112500 by National Central University, Wiley Online Library on [30/12/2024]. See the Terms and Conditions (https://onlinelibrary.wiley.com/terms-and-conditions) on Wiley Online Library for rules of use; OA articles are governed by the applicable Creative Commons License

19448007, 2024, 24, Downloaded from https://agupubs.onlinelibrary.wiley.com/doi/10.1029/2024GL112500 by National Central University, Wiley Online Library on [30/12/2024]. See the Terms and Conditions (https://onlinelibrary.wiley.com/terms-and-conditions) on Wiley Online Library for rules of use; OA articles are governed by the applicable Creative Commons License

et al., 2010; Fournier et al., 2009; Ji et al., 2017; Walwer et al., 2016). Based on these findings, we employed a data-adaptive method known as Multichannel Singular Spectrum Analysis (MSSA) to extract underlying cyclical and primary signals from noisy GPS time series. In the following sections, we first outline the MSSA methodology applied to three-component time series data from six GPS stations in the TVG. Two episodes of spatially and temporally correlated transient deformation were identified, and potential mechanisms for these events were investigated using seismic and geochemical evidence. These results provide insight into the correlation between spatiotemporal variations in transient deformation and volcanic processes in the TVG.

2. Methods and GPS Data

Multichannel Singular Spectrum Analysis (MSSA) is a data-adaptive, non-parametric technique that analyzes multiple time series (channels) simultaneously, utilizing their spatiotemporal correlations to extract common signal components, which can be categorized into trends, oscillatory patterns, and noise (Ghil et al., 2002; Groth & Ghil, 2015). Several studied have shown that MSSA can efficiently extract transient and seasonal signals from noisy data sets, enabling the identification of spatially coherent deformation patterns in GNSS networks (e.g., Walwer et al., 2016, 2022; Zhang et al., 2017). We briefly explained the MSSA methodology in Text S1 in Supporting Information S1, and refer readers to Ghil et al. (2002), Groth and Ghil (2011), and Walwer et al. (2016) for detailed information.

The current GPS network in TVG includes 14 operational GPS stations, and we selected six of these with the longest overlapping observation periods, from March 2013 to April 2021 (Figure 1). This results in a total of 18 time series (channels), each comprising 2,946 daily coordinate solutions processed with the GipsyX software package and the Precise Point Positioning technique (Bertiger et al., 2020; Zumberge et al., 1997). See Text S1 in Supporting Information S1 for more information on our GPS data processing.

Before conducting MSSA, we applied the least-squares method to detrend each coordinate time series for removing the secular trend and known offsets. We did this because secular trends represent steady-state ground deformation and usually account for most of the data variance, while offsets from earthquakes or equipment changes can interfere with time series reconstruction. By removing these components, MSSA can more effectively extract transient deformation that generally contributes less variance than the secular motion (Walwer et al., 2016). The secular motion of the six GPS stations indicates a principal strain rate of 0.18 ± 0.11 μstrain/yr, with an azimuth of ∼136° that is nearly perpendicular to the strike of the nearby Shanchiao normal fault (Figure 1).

Furthermore, GPS time series often contain gaps that can pose challenges in analyzing spatiotemporal variability using the MSSA method. To address this, we used the kSpectra Toolkit software (Ghil et al., 2002) to interpolate missing data in each time series through an iterative SSA method (Kondrashov & Ghil, 2006).

3. Transient Deformation in the TVG Area

Similar to its single channel version, SSA, MSSA begins by transforming each detrended time series into a sequence of overlapping views using a sliding window approach. The window length represents a trade-off between the amount of information extracted and its statistical significance, thus requiring careful consideration (Ghil et al., 2002). We tested four different window lengths (400, 500, 600, and 700 days) and found that they extract similar patterns of transient and periodic displacements from the 18 GPS time series (see Text S1 in Supporting Information S1). We chose a 500-day window for the following analysis, including the examination of three long-operated stations in Section 4.2.

The results of our MSSA revealed that the first four spectra are notably larger than the others, accounting for the majority of the data variance (∼27.1%, see Figure S3a in Text S1 in Supporting Information S1). The waveform and power spectrum of their associated spatiotemporal principal components (ST-PCs) show that the second and third components correspond to oscillations with an annual period, while the first and fourth components exhibit temporal variations associated with longer-term trends (see Figure S3b in Text S1 in Supporting Information S1). Given that color noise in GPS time series can lead to incorrect extraction of deformation signals, we employed a Monte Carlo SSA method (MC-SSA, Groth & Ghil, 2015) to test the statistical significance of these ST-PCs against hypothesized noise models. The results indicate that these components can be significantly

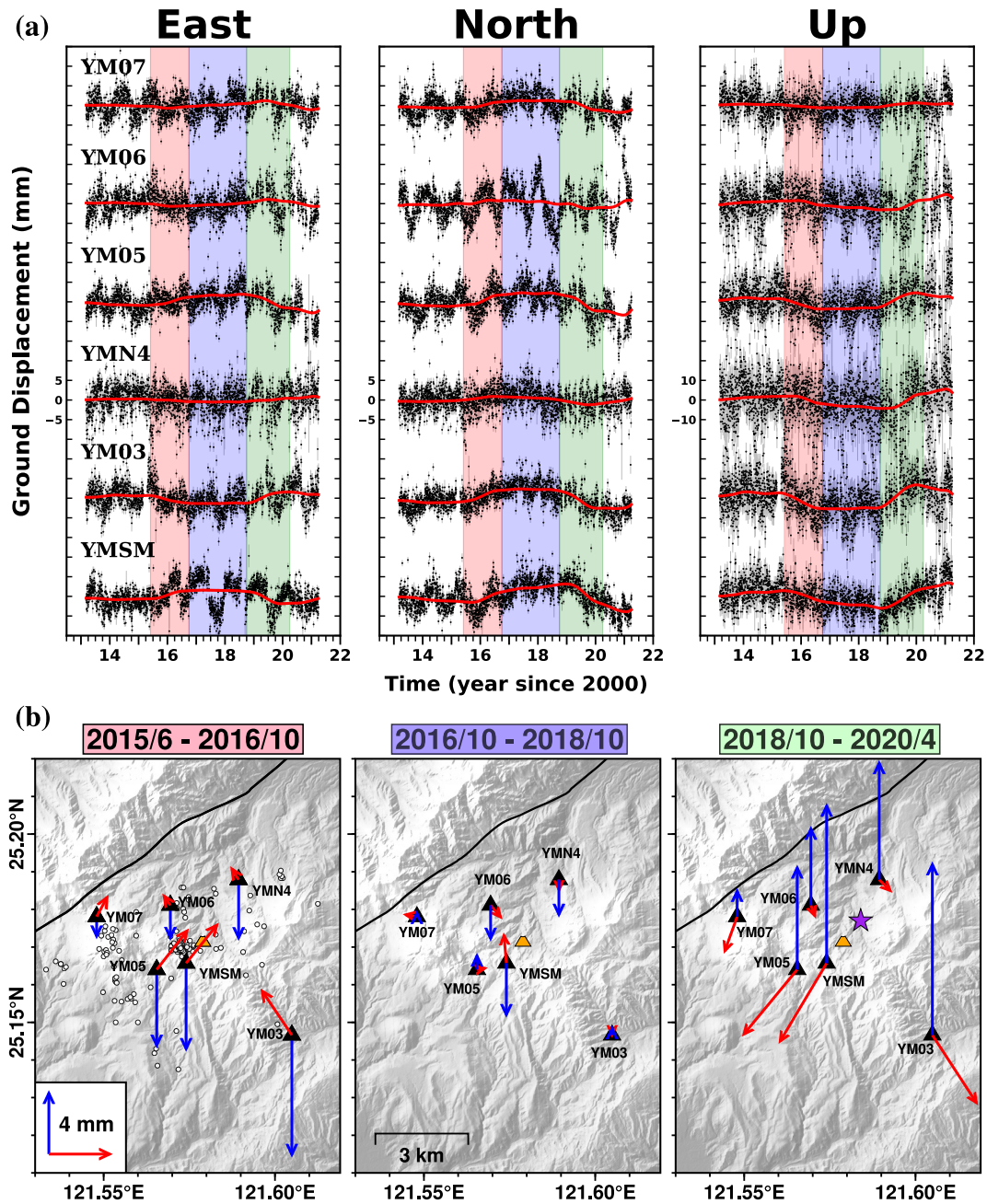

Figure 2. (a) The detrended time series (black dots) and the sum of the first and fourth reconstruction components from MSSA (red lines). (b) Ground displacements of the three time periods shown by the colored shades in (a). Red and blue arrows represent horizontal and vertical components, respectively. White circles in the leftmost subplot show April–June 2015 seismicity (Peak 3), and the purple star in the rightmost subplot labels the earthquake cluster in January 2019 (Peak 4). Orange triangles mark the Dayoukeng fumarole.

distinguished from the hypothesized white-plus-power-law noise. See Text S1 in Supporting Information S1 for detailed descriptions and figures.

Accordingly, we identified ST-PCs 1 and 4 as the major contributors to transient deformation in the TVG area, accounting for ∼14.4% of the total variance. Figure 2a displays the detrended three-component time series overlaid with the corresponding reconstruction components, RC1 and RC4. Two periods of distinct transient deformation can be identified, with the spatial patterns of horizontal and vertical motions illustrated in Figure 2b.

19448007, 2024, 24, Downloaded from https://agupubs.onlinelibrary.wiley.com/doi/10.1029/2024GL112500 by National Central University, Wiley Online Library on [30/12/2024]. See the Terms and Conditions (https://onlinelibrary.wiley.com/terms-and-conditions) on Wiley Online Library for rules of use; OA articles are governed by the applicable Creative Commons License

19448007, 2024, 24, Downloaded from https://agupubs.onlinelibrary.wiley.com/doi/10.1029/2024GL112500 by National Central University, Wiley Online Library on [30/12/2024]. See the Terms and Conditions (https://onlinelibrary.wiley.com/terms-and-conditions) on Wiley Online Library for rules of use; OA articles are governed by the applicable Creative Commons License

The first episode (EP1) occurred from June 2015 to October 2016, during which the six GPS stations experienced overall ground subsidence of up to ∼8 mm and asymmetric inward horizontal motion. After a period of relatively low deformation (<2 mm) over the next two years, the second transient episode (EP2) began in October 2018, which was characterized by ground uplift of up to ∼10 mm and asymmetric outward horizontal motion, representing a nearly reversed deformation pattern compared to EP1.

4. Discussion

Many studies have shown that water mass redistribution in the shallow crust can induce the transient ground movements observed in GNSS time series (e.g., Argus et al., 2014; Hsu et al., 2020). While the TVG area has received significant annual precipitation, often exceeding 4,000 mm, comparisons between our MSSA-filtered GPS vertical time series and local rain gauge data reveal a pattern contrary to the expected elastic response of ground motion to surface water loading (see Text S3 in Supporting Information S1). Specifically, periods of decreasing rainfall coincided with subsidence (2015–2017), while increasing rainfall was associated with uplift (2019–2021, details). This suggests that rainfall is unlikely to be the primary driver of the observed transient ground deformation during our study period.

Multiple lines of evidence, including gas composition (Lee et al., 2008), gravity changes (Lien et al., 2022; Mouyen et al., 2016), magnetotellurics (Komori et al., 2014), and seismic surveys (Y.-C. Huang et al., 2017; Lin et al., 2020), reveal prominent shallow hydrothermal systems associated with active volcanism in the TVG, particularly around the Dayoukeng fumarole and Mt. Cising (Figure 1). Moreover, high-resolution seismic tomography and relocated earthquakes from Pu, Lin, Lai, et al. (2020) suggest the presence of a shallow (∼2 km) hydrothermal reservoir and a pathway for the vertical migration of volcanic fluids beneath Dayoukeng. Given the substantial ground deformation observed around the Dayoukeng area, particularly at stations YMSM, YM05, and YMN4 (Figure 2b), we will focus in the following sections on potential volcanic activities that may be linked to these transient motions.

4.1. Potential Volcanic Processes for Transient Deformations

Pu et al. (2021a) proposed a working model for the driving mechanisms of volcanic fluids ascending beneath Dayoukeng, based on spatiotemporal variations in earthquake focal mechanisms and fumarolic gas compositions (Figures 3b and 3c). The model assumes a pre-existing volcanic conduit at a depth of 2–4 km, sealed by cap-rocks and serving as a pathway for the migration of magmatic fluids from greater depths. As these fluids ascend along the conduit, the increasing internal pressure can induce horizontal compressional stress in the surrounding rocks, promoting reverse-faulting earthquakes. This phase is followed by the increase in shallow (<2 km) normal-faulting events, as the arching cap-rocks caused by fluid accumulation can induce sub-vertical compressional stress in the overlying layer. When subjected to excessive stress, the cap-rocks may fracture, allowing the discharge of magmatic fluids and leading to an increase in the ratio of total sulfur to carbon dioxide (S_t/CO_2) in the gases ultimately emitted at the surface.

While the model was informed by two periods of data, January 2014 to June 2015 and June 2015 to July 2016 (Pu et al., 2021a), a notably high ratio of shallow normal faulting earthquakes and S_t/CO_2 from July–December 2014 was closely followed by the onset of EP1 (Figure 3). Additionally, a later increase in normal seismicity during the second half of 2015 likely contributed to further fracturing of the shallow crust beneath Dayoukeng, leading to even greater gas release, as evidenced by the peak of S_t/CO_2, and ground subsidence in 2016. These temporal correlations suggest that the pressure and volume changes in the volcanic conduit system beneath Dayoukeng may cause transient ground movements in the area.

To investigate this further, we conducted a simple modeling study of a pressurized source beneath Dayoukeng. Assuming a shallow source based on Pu, Lin, Hsu, et al. (2020), we used data only from three near-field stations (YMSM, YM05, and YMN4), which exhibit prominent transient motions, to perform a grid search for the optimal depth and pressure change that minimizes data misfit (details in Text S2 in Supporting Information S1). The results demonstrate that a single vertical prolate with a depth range of 2–4 km is a plausible conduit model for the observed transient displacements in both EP1 (a decompression of ∼120 bar) and EP2 (a compression of ∼150 bar) periods. Alternatively, a point source model at a depth of ∼2 km, which accommodates the shallow hydrothermal reservoir near the top of the conduit, as indicated by Lin et al. (2020) and Pu, Lin, Hsu, et al. (2020),

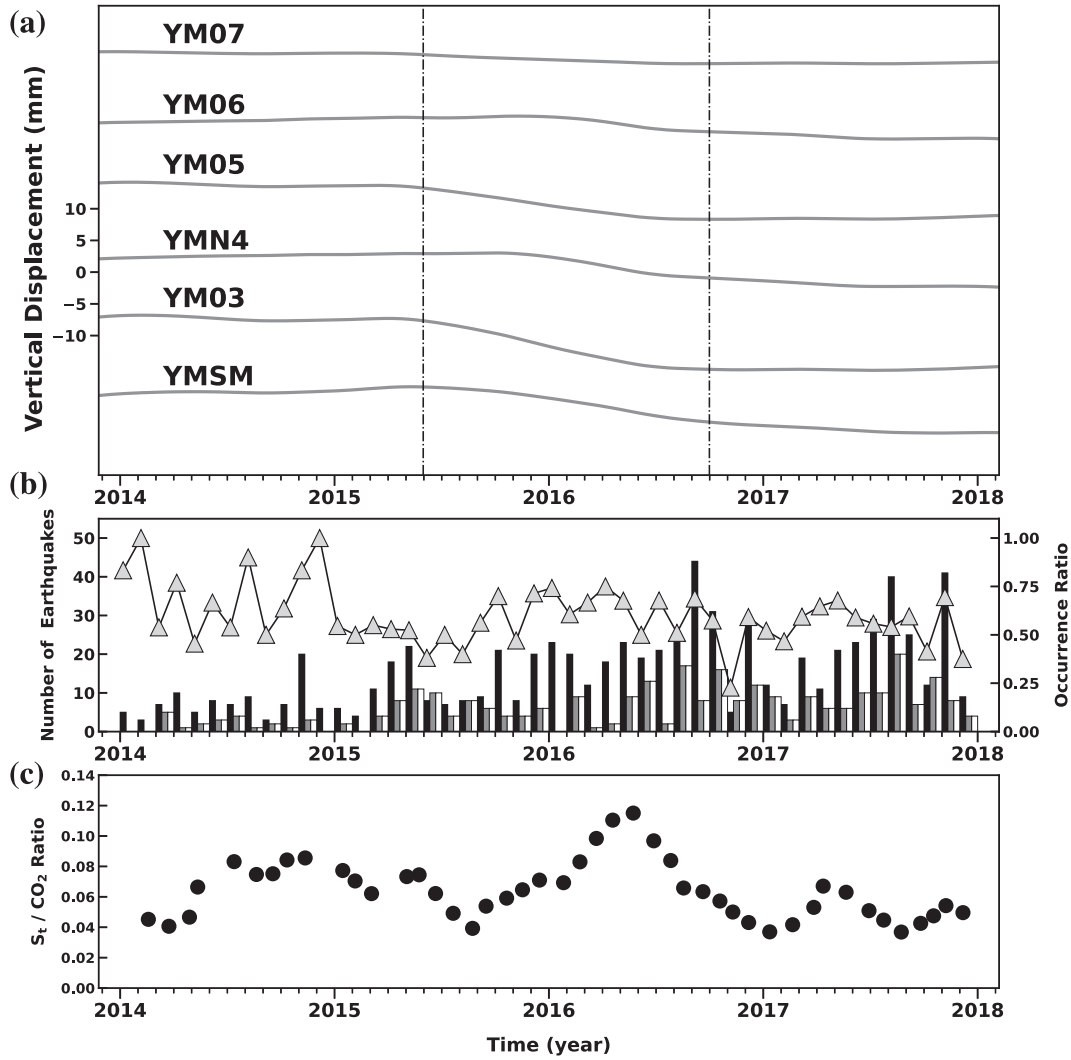

Figure 3. Temporal variations of geodetic, seismic, and geochemical measurements in the Dayoukeng area. (a) Vertical ground displacements from GPS (red lines in Figure 2a). (b) Black, gray, and white histograms show monthly earthquake numbers of shallow (<2 km) normal, reverse, and strike-slip earthquakes, and gray triangles represent the ratio of normal-type earthquakes to the total number of all earthquake types (relocating catalog from Pu et al., 2021b). (c) The ratio of total sulfur to carbon dioxide (S_t/CO_2) in the gases emitted at the surface (data from Pu et al., 2021b).

fits the data almost equally well. These findings suggest a consistency between our geodetic data and the proposed working models established through geophysical and geochemical measurements.

Apart from systematic vertical motions observed during the two transient episodes, the asymmetric horizontal movements and the significant transient displacement at YM03, which is located farther southeast of Dayoukeng, suggest that complex subsurface sources are responsible for the surface deformation. The Shanchiao normal fault crossing the TVG area, for example, shows a strong connection with the volcanism, as all active volcanic features–such as hot springs, fumaroles, and volcanic earthquakes–are confined to the hanging-wall. Lin et al. (2020), based on seismic images from ambient noise and a local dense array, proposed that fracture zones associated with the fault can allow magmatic fluids ascending from a deep crustal reservoir to feed extensive shallow hydrothermal systems beneath the TVG. While no active fumarole was identified near YM03, potential interactions among widespread subsurface hydrothermal systems or other unknown fault activities suggest the need for multi-source models. These models, not employed in this study due to limited geodetic data, can help explain the complex deformation patterns observed in the TVG.

19448007, 2024, 24, Downloaded from https://agupubs.onlinelibrary.wiley.com/doi/10.1029/2024GL112500 by National Central University, Wiley Online Library on [30/12/2024]. See the Terms and Conditions (https://onlinelibrary.wiley.com/terms-and-conditions) on Wiley Online Library for rules of use; OA articles are governed by the applicable Creative Commons License

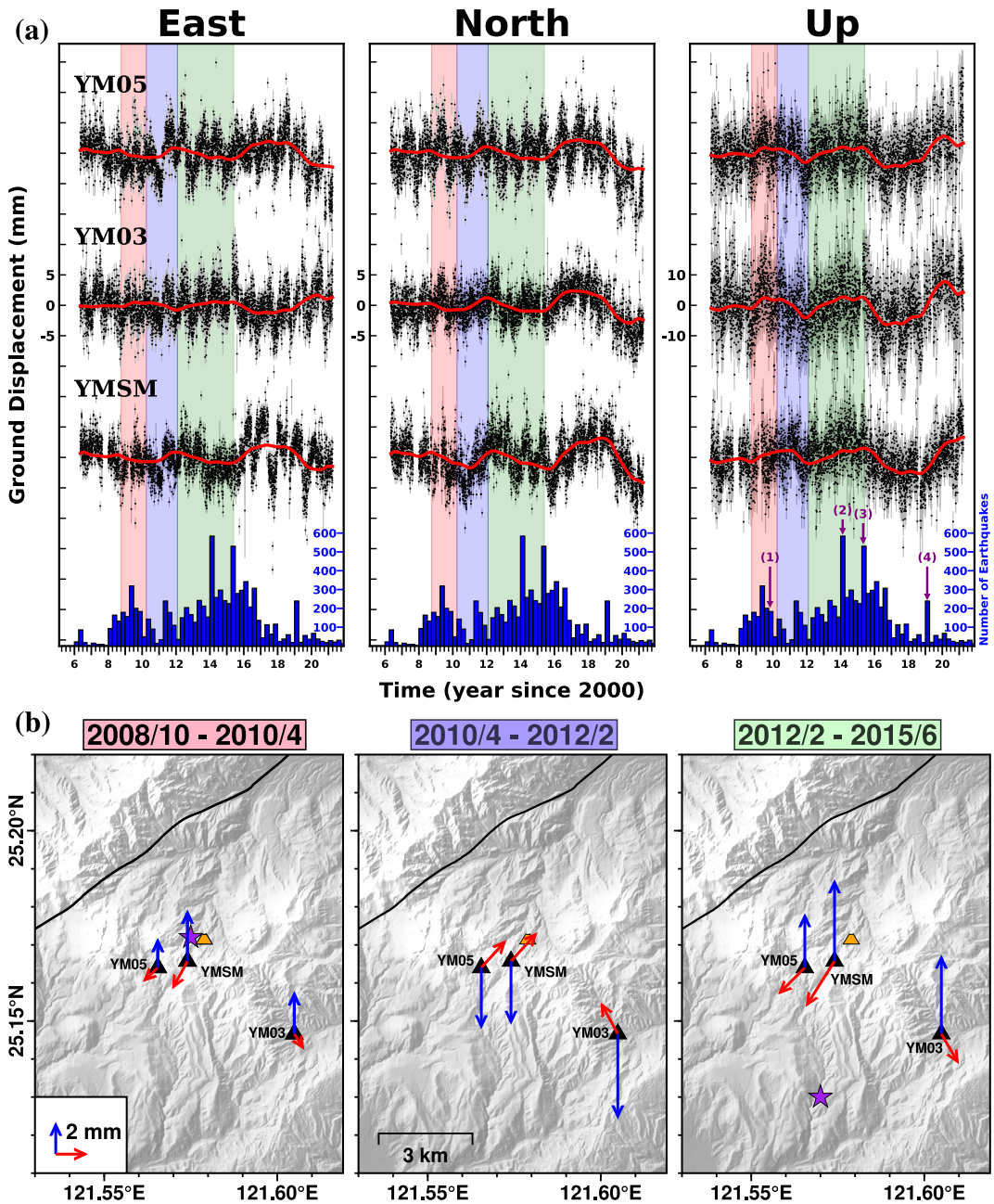

Figure 4. (a) The detrended time series (black dots) and the sum of the first two MSSA reconstruction components of the three long-operating GPS stations (red lines). Blue histograms show earthquake counts every 3 months in the area (nonrelocated catalog from TVO), with the four peaks described in the main text. (b) Ground displacements of the three time periods shown by the colored shades in (a). Red and blue arrows represent horizontal and vertical components, respectively. Purple stars label earthquake clusters in October 2009 (Peak 1, the leftmost subplot) and February 2014 (Peak 2, the rightmost subplot). Orange triangles mark the Dayoukeng fumarole.

4.2. Spatiotemporal Variations in TVG Deformation and Seismicity

To investigate whether the TVG had experienced other similar deformation cycles as outlined earlier, we applied MSSA to the time series from three long-operating GPS stations, YM03, YM05, and YMSM (see Texts S1–S5 in Supporting Information S1 for details). Figure 4a displays the detrended time series and their primary transient signals (the sum of the first two RCs), from which the aforementioned 2015–2020 transient episode as shown in Figure 2 can be clearly identified. Additionally, similar deformation patterns are observed

19448007, 2024, 24, Downloaded from https://agupubs.onlinelibrary.wiley.com/doi/10.1029/2024GL112500 by National Central University, Wiley Online Library on [30/12/2024]. See the Terms and Conditions (https://onlinelibrary.wiley.com/terms-and-conditions) on Wiley Online Library for rules of use; OA articles are governed by the applicable Creative Commons License

19448007, 2024, 24, Downloaded from https://agupubs.onlinelibrary.wiley.com/doi/10.1029/2024GL112500 by National Central University, Wiley Online Library on [30/12/2024]. See the Terms and Conditions (https://onlinelibrary.wiley.com/terms-and-conditions) on Wiley Online Library for rules of use; OA articles are governed by the applicable Creative Commons License

at the three stations (Figure 4b), including: (a) uplift and outward motion from October 2008 to April 2010; (b) subsidence and inward motion from April 2010 to February 2012; and (c) another phase of uplift and outward motion from February 2012 to June 2015, which occurred right before EP1 shown in Figure 2. Although the amplitudes of these displacements, approximately 2–3 mm in horizontal and ∼3–5 mm in vertical, are significantly lower than those observed during the 2015–2020 transient episode, the MSSA-filtered time series clearly demonstrate the spatial and temporal repeatability of deformation cycles in the TVG area, at least near Dayoukeng.

Deformation cycles, typically characterized by periods of ground uplift and subsidence, have been observed in numerous volcanic systems worldwide, and variations in these cycles often correlate with changes in local seismicity (e.g., Hill et al., 2003; Smith et al., 2009). Accordingly, we investigated the temporal distribution of earthquakes from 2006 to 2021 in the TVG area. As shown in Figure 4a, three notable peaks in shallow earthquakes (depths <4 km) around the Dayoukeng area likely occurred concurrently with changes in deformation episodes. Peaks 1 and 3 correspond to earthquake swarms in October 2009 (Pu et al., 2014) and April–June 2015 (Pu et al., 2021a), respectively. Pu et al. (2014) attributed the October 2009 swarm to active volcanism, citing its high b-value of 2.17 and the presence of pipe-like seismic zone. Peak 4, moreover, includes ∼170 shallow events in January 2019, clustered in a fumarole area just ∼1 km north of Dayoukeng (Figure 1). Although additional evidence, such as geochemical data, is lacking, these correlations suggest that hydrothermal and volcanic processes beneath Dayoukeng may have driven spatially and temporally consistent variations in seismicity and deformation patterns in the area.

Peak 2, on the other hand, includes relatively deep earthquakes (3–6 km) located southeast of Mt. Shamao, one of the latest eruptive units in TVG with low hydrothermal activity (Figure 1). This peak features a magnitude 4.2 earthquake in 12 February 2014–the second largest in TVG since 1900–and subsequent seismicity mostly occurred afterward. While this peak was immediately followed by a minor bump in the MSSA-filtered GPS time series (Figure 4a), overall deformation trends remained steady from 2012 to 2015. Pu et al. (2017) proposed that this earthquake sequence resulted from a combined synergistic effect of a collapsed reservoir filled with volcanic fluids and faulting activities along the Shanchiao fault, a mechanism distinct from the three Dayoukeng clusters mentioned above.

5. Conclusions

This is the first study to analyze transient ground deformation using continuous GPS records and to examine their spatiotemporal relationship with seismic and geochemical observations of the Tatun Volcanic Group. By applying MSSA to extract primary trend variations from noisy time series of six GPS stations spanning 2006 to 2021, we identified several episodes of subsidence and uplift, along with asymmetric horizontal motions directed inward and outward toward Dayoukeng, the largest fumarole and hydrothermal area in TVG. Notably, three earthquake clusters near Dayoukeng occurred around the same time as changes between deformation episodes. The most significant of these, the initiation of subsidence in June 2015, is well explained by a hydrothermal conduit model, supported by evidence from seismic focal mechanism, gas composition, and simple pressurized source models. Our findings suggest that hydrothermal and volcanic processes beneath the TVG may have driven spatiotemporally consistent variations in seismicity and deformation patterns in the area, similar to those observed in many other volcanic systems worldwide.

Data Availability Statement

The GPS time series data of the six TVO stations are available at Y. S. Huang et al. (2024). Both focal mechanisms and the St/CO_2 ratio data can be accessed at Pu et al. (2021b). Maps were created through PyGMT (Uieda et al., 2021) using Generic Mapping Tools (GMT) version 6 (Wessel et al., 2019).

Acknowledgments
The authors thank the Taiwan Volcano Observatory at Tatun (TVO) for providing GPS and earthquake data. Insightful comments from an anonymous reviewer greatly improve this manuscript. This research was funded by the National Science and Technology Council of Taiwan under Grant NSTC 111-2116-M-008-013.

References

Argus, D. F., Fu, Y., & Landerer, F. W. (2014). Seasonal variation in total water storage in California inferred from GPS observations of vertical land motion. *Geophysical Research Letters*, *41*(6), 1971–1980. https://doi.org/10.1002/2014GL059570

Bertiger, W., Bar-Sever, Y., Dorsey, A., Haines, B., Harvey, N., Hemberger, D., et al. (2020). GipsyX/RTGx, a new tool set for space geodetic operations and research. *Advances in Space Research*, *66*(3), 469–489. https://doi.org/10.1016/j.asr.2020.04.015

Bos, M. S., Fernandes, R. M. S., Williams, S. D. P., & Bastos, L. (2013). Fast error analysis of continuous GNSS observations with missing data. *Journal of Geodesy*, *87*(4), 351–360. https://doi.org/10.1007/s00190-012-0605-0

Chang, W.-L., Smith, R. B., Farrell, J., & Puskas, C. M. (2010). An extraordinary episode of Yellowstone caldera uplift, 2004–2010, from GPS and InSAR observations. *Geophysical Research Letters*, *37*(23). https://doi.org/10.1029/2010GL045451

Chang, W.-L., Wang, C.-C., Chiu, C.-Y., & Rau, R.-J. (2017). Interseismic crustal deformation of the Northern Taiwan from GPS and InSAR. In *Abstract T53C-08 presented at 2017 fall meeting, AGU, New Orleans, LA, 11-15 Dec*.

Chen, W.-S., Yang, C.-C., Yang, H.-C., Liu, J.-K., Chan, Y.-C., Shieh, K.-S., & Hsieh, Y.-C. (2007). Scanning laser mapping (2Mx2M DTM) of the Pleistocene Tatun volcanic landform. *Bulletin of the Central Geological Survey*, *20*, 101–128. (in Chinese with English abstract).

Fournier, T., Freymueller, J., & Cervelli, P. (2009). Tracking magma volume recovery at Okmok volcano using GPS and an unscented Kalman filter. *Journal of Geophysical Research*, *114*(B2), B02405. https://doi.org/10.1029/2008JB005837

Ghil, M., Allen, M. R., Dettinger, M. D., Ide, K., Kondrashov, D., Mann, M. E., et al. (2002). Advanced spectral methods for climatic time series. *Reviews of Geophysics*, *40*(1), 3-1-3–41. https://doi.org/10.1029/2000RG000092

Groth, A., & Ghil, M. (2011). Multivariate singular spectrum analysis and the road to phase synchronization. *Physical Review E*, *84*(3), 036206. https://doi.org/10.1103/PhysRevE.84.036206

Groth, A., & Ghil, M. (2015). Monte Carlo singular spectrum analysis (SSA) revisited: Detecting oscillator clusters in multivariate datasets. *Journal of Climate*, *28*(19), 7873–7893. https://doi.org/10.1175/JCLI-D-15-0100.1

Hill, D. P., Langbein, J. O., & Prejean, S. (2003). Relations between seismicity and deformation during unrest in Long Valley Caldera, California, from 1995 through 1999. *Journal of Volcanology and Geothermal Research*, *127*(3), 175–193. https://doi.org/10.1016/S0377-0273(03)00169-0

Hsu, Y.-J., Fu, Y., Bürgmann, R., Hsu, S.-Y., Lin, C.-C., Tang, C.-H., & Wu, Y.-M. (2020). Assessing seasonal and interannual water storage variations in Taiwan using geodetic and hydrological data. *Earth and Planetary Science Letters*, *550*, 116532. https://doi.org/10.1016/j.epsl.2020.116532

Huang, Y.-S., Chang, W.-L., Pu, H.-C., Chiu, C.-Y., Lai, Y.-C., & Shih, M.-H. (2024). GPS position time series data for the Tatun Volcano Group (TVG) region [Dataset]. *Zenodo*. https://doi.org/10.5281/zenodo.13770622

Huang, Y.-C., Lin, C.-H., & Kagiyama, T. (2017). Shallow crustal velocities and volcanism suggested from ambient noise studies using a dense broadband seismic network in the Tatun Volcano Group of Taiwan. *Journal of Volcanology and Geothermal Research*, *341*, 6–20. https://doi.org/10.1016/j.jvolgeores.2017.05.016

Huang, H.-H., Wu, E.-S., Lin, C.-H., Ko, J. Y.-T., Shih, M.-H., & Koulakov, I. (2021). Unveiling Tatun volcanic plumbing structure induced by post-collisional extension of Taiwan mountain belt. *Scientific Reports*, *11*(1), 5286. https://doi.org/10.1038/s41598-021-84763-z

Ji, K. H., Yun, S.-H., & Rim, H. (2017). Episodic inflation events at Akutan Volcano, Alaska, during 2005–2017. *Geophysical Research Letters*, *44*(16), 8268–8275. https://doi.org/10.1002/2017GL074626

Komori, S., Utsugi, M., Kagiyama, T., Inoue, H., Chen, C.-H., Chiang, H.-T., et al. (2014). Hydrothermal system in the Tatun Volcano Group, northern Taiwan, inferred from crustal resistivity structure by audio-magnetotellurics. *Progress in Earth and Planetary Science*, *1*(1), 20. https://doi.org/10.1186/s40645-014-0020-7

Kondrashov, D., & Ghil, M. (2006). Spatio-temporal filling of missing points in geophysical data sets. *Nonlinear Processes in Geophysics*, *13*(2), 151–159. https://doi.org/10.5194/npg-13-151-2006

Langbein, J. (2017). Improved efficiency of maximum likelihood analysis of time series with temporally correlated errors. *Journal of Geodesy*, *91*(8), 985–994. https://doi.org/10.1007/s00190-017-1002-5

Lee, H.-F., Yang, T. F., Lan, T. F., Chen, C.-H., Song, S.-R., & Tsao, S. (2008). Temporal variations of gas compositions of fumaroles in the Tatun Volcano Group, northern Taiwan. *Journal of Volcanology and Geothermal Research*, *178*(4), 624–635. https://doi.org/10.1016/j.jvolgeores.2008.06.005

Lien, T., Chang, E. T., Hwang, C., Cheng, C.-C., Chen, R.-F., & Mu, C.-H. (2022). Delineating a volcanic aquifer using groundwater-induced gravity changes in the Tatun Volcano Group, Taiwan. *Terrestrial, Atmospheric and Oceanic Sciences*, *33*(1), 31. https://doi.org/10.1007/s44195-022-00031-1

Lin, C.-H. (2016). Evidence for a magma reservoir beneath the Taipei metropolis of Taiwan from both S-wave shadows and P-wave delays. *Scientific Reports*, *6*(1), 39500. https://doi.org/10.1038/srep39500

Lin, C. H., Lai, Y. C., Shih, M. H., Lin, C. J., Ku, J. S., & Huang, Y. C. (2020). A major hydrothermal reservoir underneath the Tatun Volcano Group of Taiwan: Clues from a dense linear geophone array. *Pure and Applied Geophysics*, *177*(6), 2889–2902. https://doi.org/10.1007/s00024-019-02396-w

Mouyen, M., Chao, B. F., Hwang, C., & Hsieh, W.-C. (2016). Gravity monitoring of Tatun Volcanic Group activities and inference for underground fluid circulations. *Journal of Volcanology and Geothermal Research*, *328*, 45–58. https://doi.org/10.1016/j.jvolgeores.2016.10.001

Murase, M., Lin, C.-H., Kimata, F., Mori, H., & Pu, H.-C. (2014). Volcano-hydrothermal activity detected by precise levelling surveys at the Tatun volcano group in Northern Taiwan during 2006–2013. *Journal of Volcanology and Geothermal Research*, *286*, 30–40. https://doi.org/10.1016/j.jvolgeores.2014.09.001

Nikolaidis, R. (2002). Observation of geodetic and seismic deformation with the Global Positioning System Ph.D. dissertation. Univ. of Calif., San Diego, La Jolla.

Pu, H.-C., Lin, C.-H., Chang, L.-C., Kan, C.-W., Lin, C.-M., Li, Y.-H., et al. (2017). Geological implications of the 0212 earthquake in 2014 at the Tatun Volcano Group of Taiwan: Synergistic effects of volcanic and faulting activities. *Journal of Asian Earth Sciences*, *149*, 93–102. https://doi.org/10.1016/j.jseaes.2017.08.021

Pu, H.-C., Lin, C.-H., Hsu, Y.-J., Lai, Y.-C., Shih, M.-H., Murase, M., & Chang, L.-C. (2020). Volcano-hydrothermal inflation revealed through spatial variation in stress field in Tatun Volcano Group, Northern Taiwan. *Journal of Volcanology and Geothermal Research*, *390*, 106712. https://doi.org/10.1016/j.jvolgeores.2019.106712

Pu, H. C., Lin, C. H., Lai, Y. C., Shih, M. H., Chang, L. C., Lee, H. F., et al. (2020). Active volcanism revealed from a seismicity conduit in the long-resting Tatun Volcano Group of northern Taiwan. *Scientific Reports*, *10*(1), 6153. https://doi.org/10.1038/s41598-020-63270-7

Pu, H.-C., Lin, C.-H., Huang, Y.-C., Chang, L.-C., Lee, H.-F., Leu, P.-L., et al. (2014). The volcanic earthquake swarm of October 20, 2009 in the Tatun Area of Northern Taiwan. *Terrestrial, Atmospheric and Oceanic Sciences*, *25*(5), 625–635. https://doi.org/10.3319/TAO.2014.04.11.02(T)

Pu, H.-C., Lin, C.-H., Lee, H.-F., Lai, Y.-C., Chang, L.-C., & Shih, M.-H. (2021a). Ascending volcanic fluids portended by spatiotemporal variations of the earthquake mechanisms in the Tatun Volcano Group in Northern Taiwan. *Geophysical Research Letters*, *48*(9), e2020GL091686. https://doi.org/10.1029/2020GL091686

Pu, H.-C., Lin, C.-H., Lee, H.-F., Lai, Y.-C., Chang, L.-C., & Shih, M.-H. (2021b). Supplemental data (FPS & St/CO2) and parameters of HypoDD @ TVG [Dataset]. *Mendeley Data, V1*. https://doi.org/10.17632/c5kt45k5y6.1

19448007, 2024, 24, Downloaded from https://agupubs.onlinelibrary.wiley.com/doi/10.1029/2024GL112500 by National Central University, Wiley Online Library on [30/12/2024]. See the Terms and Conditions (https://onlinelibrary.wiley.com/terms-and-conditions) on Wiley Online Library for rules of use; OA articles are governed by the applicable Creative Commons License

Smith, R. B., Jordan, M., Steinberger, B., Puskas, C. M., Farrell, J., Waite, G. P., et al. (2009). Geodynamics of the Yellowstone hotspot and mantle plume: Seismic and GPS imaging, kinematics, and mantle flow. *Journal of Volcanology and Geothermal Research*, *188*(1), 26–56. https://doi.org/10.1016/j.jvolgeores.2009.08.020

Tung, H., Chen, H.-Y., Hu, J.-C., Ching, K.-E., Chen, H., & Yang, K.-H. (2016). Transient deformation induced by groundwater change in Taipei metropolitan area revealed by high resolution X-band SAR interferometry. *Tectonophysics*, *692*, 265–277. https://doi.org/10.1016/j.tecto.2016.03.030

Uieda, L., Tian, D., Leong, W. J., Toney, L., Schlitzer, W., Yao, J., et al. (2021). PyGMT: A Python interface for the generic mapping tools (v0.3.1) [Software]. *Zenodo*. https://doi.org/10.5281/zenodo.4592991

Walwer, D., Calais, E., & Ghil, M. (2016). Data-adaptive detection of transient deformation in geodetic networks. *Journal of Geophysical Research: Solid Earth*, *121*(3), 2129–2152. https://doi.org/10.1002/2015JB012424

Walwer, D., Ghil, M., & Calais, E. (2022). A data-based minimal model of episodic inflation events at volcanoes. *Frontiers in Earth Science*, *10*. https://doi.org/10.3389/feart.2022.759475

Wessel, P., Luis, J. F., Ueda, L., Scharroo, R., Wobbe, F., Smith, W. H. F., & Tian, D. (2019). The generic mapping tools version 6 [Software]. *Zenodo*, *20*(11), 5556–5564. (Funded by US National Science Foundation grants OCE-1558403 and EAR-1829371). https://doi.org/10.5281/zenodo.3407866

Yang, T., Sano, Y., & Song, S. (1999). 3He/4He ratios of fumaroles and bubbling gases of hot springs in Tatun Volcano Group, North Taiwan. *Il Nuovo Cimento - B C*, *22*, 281–286.

Zhang, B., Liu, L., Khan, S. A., van Dam, T., Zhang, E., & Yao, Y. (2017). Transient variations in glacial mass near Upernavik Isstrøm (West Greenland) detected by the combined use of GPS and GRACE data. *Journal of Geophysical Research: Solid Earth*, *122*(12), 10626–10642. https://doi.org/10.1002/2017JB014529

Zumberge, J. F., Heflin, M. B., Jefferson, D. C., Watkins, M. M., & Webb, F. H. (1997). Precise point positioning for the efficient and robust analysis of GPS data from large networks. *Journal of Geophysical Research*, *102*(B3), 5005–5017. https://doi.org/10.1029/96JB03860

References From the Supporting Information

Allen, M. R., & Robertson, A. W. (1996). Distinguishing modulated oscillations from coloured noise in multivariate datasets. *Climate Dynamics*, *12*(11), 775–784. https://doi.org/10.1007/s003820050142

Allen, M. R., & Smith, L. A. (1996). Monte Carlo SSA: Detecting irregular oscillations in the presence of colored noise. *Journal of Climate*, *9*(12), 3373–3404. https://doi.org/10.1175/1520-0442(1996)009<3373:MCSDIO>2.0.CO;2

Borsa, A. A., Agnew, D. C., & Cayan, D. R. (2014). Ongoing drought-induced uplift in the western United States. *Science*, *345*(6204), 1587–1590. https://doi.org/10.1126/science.1260279

Böhm, J., Werl, B., & Schuh, H. (2006). Troposphere mapping functions for GPS and very long baseline interferometry from European Centre for Medium-Range Weather Forecasts operational analysis data. *Journal of Geophysical Research*, *111*(B2), B02406. https://doi.org/10.1029/2005JB003629

Broomhead, D. S., & King, G. P. (1986). Extracting qualitative dynamics from experimental data. *Physica D: Nonlinear Phenomena*, *20*(2), 217–236. https://doi.org/10.1016/0167-2789(86)90031-X

Chen, C. H. (1970). Geology and geothermal power potential of the Tatun volcanic region. *Geothermics*, *2*, 1134–1143. https://doi.org/10.1016/0375-6505(70)90425-6

Davis, J. L., Wernicke, B. P., & Tamisiea, M. E. (2012). On seasonal signals in geodetic time series. *Journal of Geophysical Research*, *117*(B1), B01403. https://doi.org/10.1029/2011JB008690

Farrell, W. E. (1972). Deformation of the Earth by surface loads. *Reviews of Geophysics*, *10*(3), 761–797. https://doi.org/10.1029/RG010i003p00761

King, M. A., Watson, C. S., Penna, N. T., & Clarke, P. J. (2008). Subdaily signals in GPS observations and their effect at semiannual and annual periods. *Geophysical Research Letters*, *35*(3), L03302. https://doi.org/10.1029/2007GL032252

King, N. E., Argus, D., Langbein, J., Agnew, D. C., Bawden, G., Dollar, R. S., et al. (2007). Space geodetic observation of expansion of the San Gabriel Valley, California, aquifer system, during heavy rainfall in winter 2004–2005. *Journal of Geophysical Research*, *112*(B3), B03409. https://doi.org/10.1029/2006JB004448

Lyard, F. H., Allain, D. J., Cancet, M., Carrère, L., & Picot, N. (2021). FES2014 global ocean tide atlas: Design and performance. *Ocean Science*, *17*(3), 615–649. https://doi.org/10.5194/os-17-615-2021

Tiampo, K. F., Rundle, J. B., Fernandez, J., & Langbein, J. O. (2000). Spherical and ellipsoidal volcanic sources at Long Valley caldera, California, using a genetic algorithm inversion technique. *Journal of Volcanology and Geothermal Research*, *102*(3), 189–206. https://doi.org/10.1016/S0377-0273(00)00185-2

Vautard, R., & Ghil, M. (1989). Singular spectrum analysis in nonlinear dynamics, with applications to paleoclimatic time series. *Physica D: Nonlinear Phenomena*, *35*(3), 395–424. https://doi.org/10.1016/0167-2789(89)90077-8

Xu, C., & Yue, D. (2015). Monte Carlo SSA to detect time-variable seasonal oscillations from GPS-derived site position time series. *Tectonophysics*, *665*, 118–126. https://doi.org/10.1016/j.tecto.2015.09.029

Yan, H., Chen, W., Zhu, Y., Zhang, W., & Zhong, M. (2009). Contributions of thermal expansion of monuments and nearby bedrock to observed GPS height changes. *Geophysical Research Letters*, *36*(13), L13301. https://doi.org/10.1029/2009GL038152

Yang, X.-M., Davis, P. M., & Dieterich, J. H. (1988). Deformation from inflation of a dipping finite prolate spheroid in an elastic half-space as a model for volcanic stressing. *Journal of Geophysical Research*, *93*(B5), 4249–4257. https://doi.org/10.1029/JB093iB05p04249

19448007, 2024, 24, Downloaded from https://agupubs.onlinelibrary.wiley.com/doi/10.1029/2024GL112500 by National Central University, Wiley Online Library on [30/12/2024]. See the Terms and Conditions (https://onlinelibrary.wiley.com/terms-and-conditions) on Wiley Online Library for rules of use; OA articles are governed by the applicable Creative Commons License